Academic Journal of Science and Technology
ISSN: 2771-3032 | Vol. 14, No. 1, 2025

Pore Structure and Fractal Characteristics of the H Formation of the K Structure in the Eastern X Depression

Chong Hu[1, 2]

[1]School of Earth Sciences and Engineering, Xi'an Shiyou University, Xi'an, Shaanxi 710065, China
[2]Shaanxi Key Laboratory of Petroleum Accumulation Geology, Xi'an Shiyou University, Xi'an, Shaanxi 710065, China

Abstract: To address the limited understanding of the pore structure in the H reservoir of the K structure in the eastern X depression, a fractal analysis method was employed to analyze the reservoir pores. Through the integration of experimental techniques, including casting thin sections, X-ray diffraction, and mercury intrusion, the study identified the reservoir's pore types, pore-throat distribution characteristics, and fractal properties. Additionally, it explored the relationships between fractal dimensions, reservoir physical properties, pore structure parameters, and mineral compositions.The results indicate that the pore types in the reservoir of the study area are primarily primary intergranular pores, intergranular dissolution pores, and intragranular dissolution pores. The reservoir's mineral composition is dominated by quartz and feldspar, with chlorite being the most abundant among clay minerals.Based on the morphology of capillary pressure curves, the reservoir pore structures are classified into four types: Type I, Type II, Type III, and Type IV. Their storage capacity and permeability decrease sequentially, while heterogeneity gradually increases.The reservoir pores exhibit multifractal characteristics, with the pore space divided into macropores (megapores and macropores), mesopores, and micropores (micropores and nanopores). The pore structure of macropores and mesopores is superior to that of micropores. The fractal dimension is unrelated to reservoir porosity but shows good correlations with permeability, pore structure parameters, and mineral composition.This study reveals the pore size distribution characteristics of the reservoir from the perspective of multifractal theory, providing a basis for the development of the H reservoir in the K structure of the X depression in the eastern region.

Keywords: Pore structure; high pressure mercury injection; fractal dimension.

1. Introduction

With the continuous growth of global energy demand, low-permeability reservoirs have become a key focus in oil and gas exploration and development[1-2]. The pore structure plays a critical role in determining the seepage capacity of these reservoirs. Conducting detailed studies on the microscopic pore-throat structure of low-permeability reservoirs is essential for their proper evaluation and effective development[3-6]. Fractal theory, initially introduced by Mandelbrot in the 1970s, provides a framework for describing the structural characteristics of irregular objects in nature[7]. Previous studies have demonstrated that the microscopic pore-throat structure of sandstone exhibits strong statistical self-similarity, and that geometric fractals can effectively characterize its heterogeneity and complexity. Consequently, geometric fractals are widely employed in research on the micro-pore-throat structures of rocks[8-12].

This study focuses on the H group sandstone of the K structure within the eastern X depression. Using casting thin sections, X-ray diffraction, high-pressure mercury intrusion, and fractal theory, it explores the pore structure and its fractal dimensions. The analysis highlights the contributions of different reservoir spaces to physical properties, providing a theoretical foundation for hydrocarbon reservoir exploration and development.

2. Reservoir Characteristics

2.1. Petrological Characteristics of Reservoirs

Based on the analysis of core samples and thin sections, the H sandstone reservoir in the K structure of the eastern X depression is primarily composed of feldspathic lithic sandstone and lithic quartz sandstone, with lithic feldspathic sandstone and feldspathic quartz sandstone as secondary types (Fig.1). The quartz content ranges from 57% to 82%, with an average of 73.5%. The feldspar content ranges from 5.0% to 28.5%, with an average of 12.3%. The lithic fragment content varies between 7.5% and 28.0%, with an average of 14.1%. The lithic fragments are primarily composed of metamorphic rock fragments, followed by igneous rock fragments, with occasional sedimentary rock fragments. The interstitial materials are mainly matrix, carbonate cement, siliceous cement, and authigenic clay minerals. The clastic particles exhibit moderate sorting and rounding, with most displaying sub-angular to sub-rounded shapes.

2.2. Physical Properties of Reservoirs

Based on core physical property analysis, the porosity of the deep clastic rock reservoirs in Formation H of the K structure in the eastern X Sag ranges from 0.5% to 19.7%, with an average value of 11.6% and a median value of 10.5% (Fig.2-a). The permeability ranges from 0.057×10^{-3} μm² to 268.981×10^{-3} μm², with an average value of 6.375×10^{-3} μm² and a median value of 1.463×10^{-3} μm² (Fig.2-b).

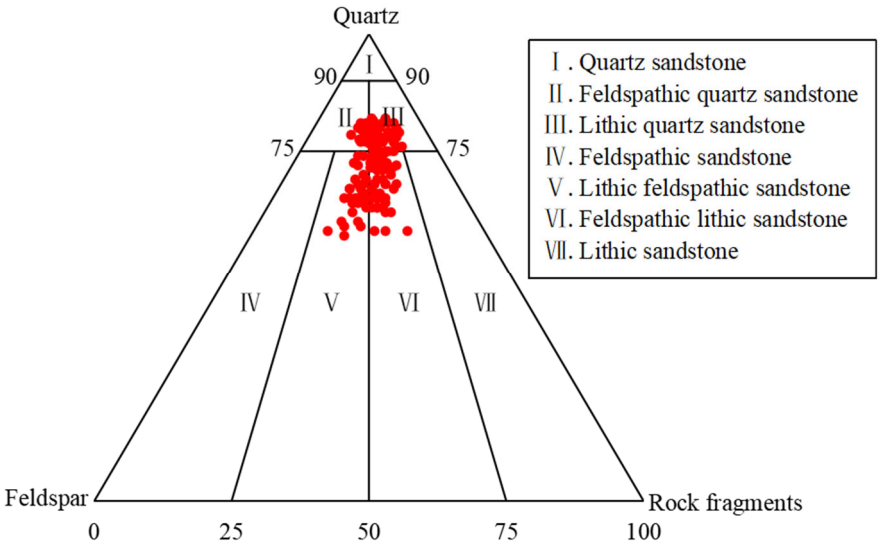

Figure 1. Triangle diagram of different rock types in the H formation of the K structure in the eastern X depression

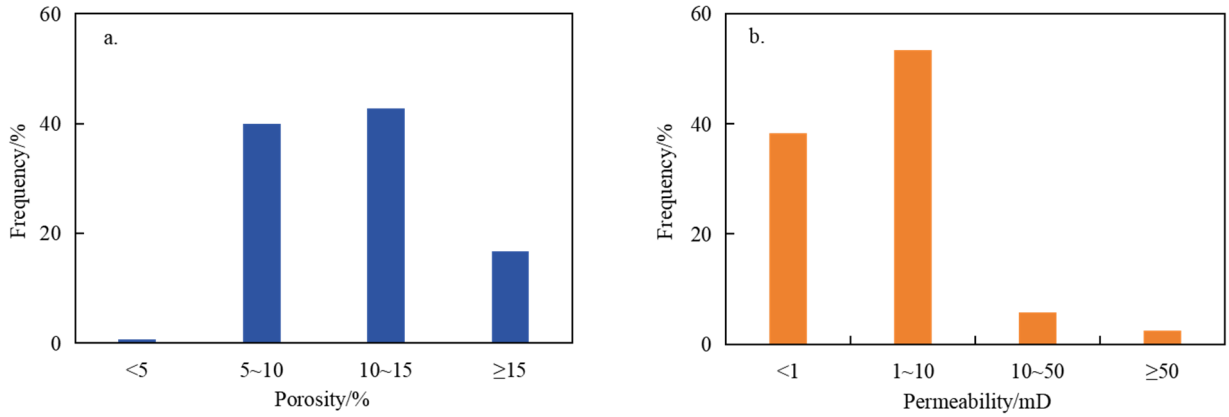

a. porosity distribution frequency diagram; b. permeability distribution frequency diagram.

Figure 2. Physical properties of sandstone reservoirs in the H formation of the K structure in the eastern X depression

3. Micro Pore-throat Characteristics

3.1. Pore Classification and Characteristics

Through microscopic identification of casting thin sections, the pore types and porosity of sandstone samples from the H Formation in the K structure of an eastern depression were identified and analyzed. The results show that the pore types of the sandstone are mainly primary pores, followed by secondary pores, with average planar porosities of 3.92% and 2.37%, respectively. Among the secondary pores, intergranular dissolution pores are the most common, with an average planar porosity of 0.92%; intragranular dissolution pores and micropores within cements follow, with average planar porosities of 0.93% and 0.39%, respectively. A small amount of moldic pores and dissolution cavities are observed, with average planar porosities of 0.09% and 0.01%, respectively (Fig.3). Under the microscope, primary pores are triangular, polygonal, or similar in shape, with straight edges and no apparent signs of dissolution (Fig.4-a). Intergranular dissolution pores exhibit irregular or polygonal shapes, with edges showing clear dissolution features (Fig.4-b). Intragranular dissolution pores are mainly formed by the localized dissolution of feldspars and easily soluble lithic fragments (Fig.4-c,4-d). Micropores within the cements consist predominantly of dissolution pores in the matrix and cement (Fig.4-e). Moldic pores, caused by the complete dissolution of localized feldspars and soluble lithic fragments, are occasionally observed (Fig.4-f). Additionally, partial dissolution cavities are visible under the microscope (Fig.4-g).

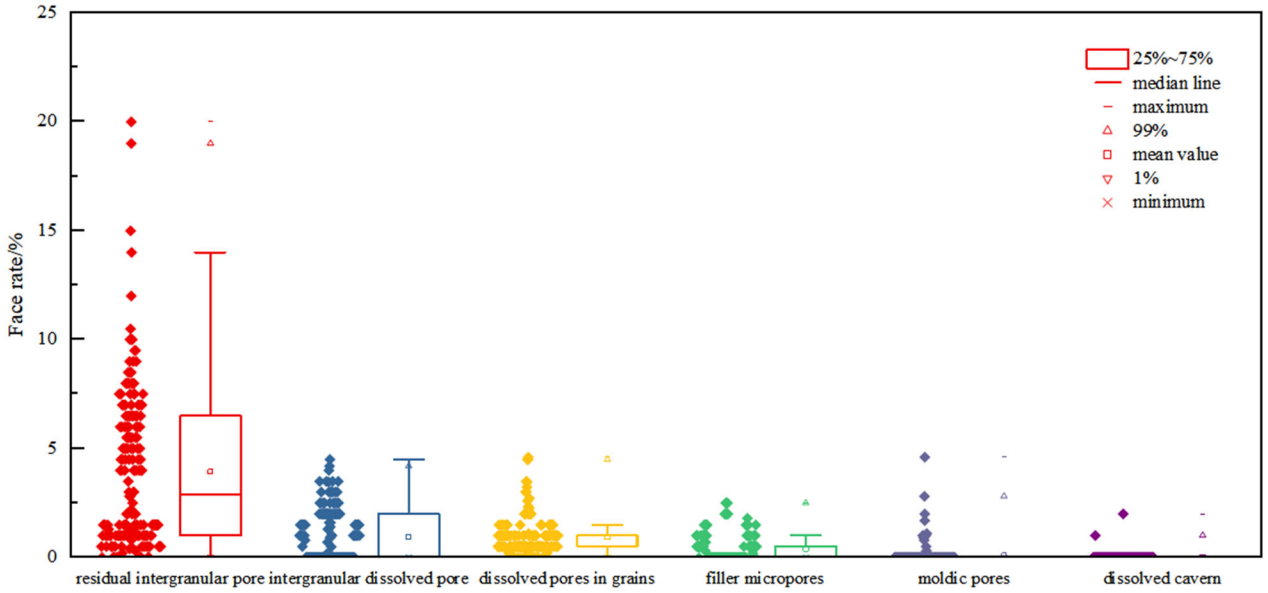

Figure 3. Box plots showing the thin-section porosity of pores occurred in the H formation of the K structure in the eastern X depression

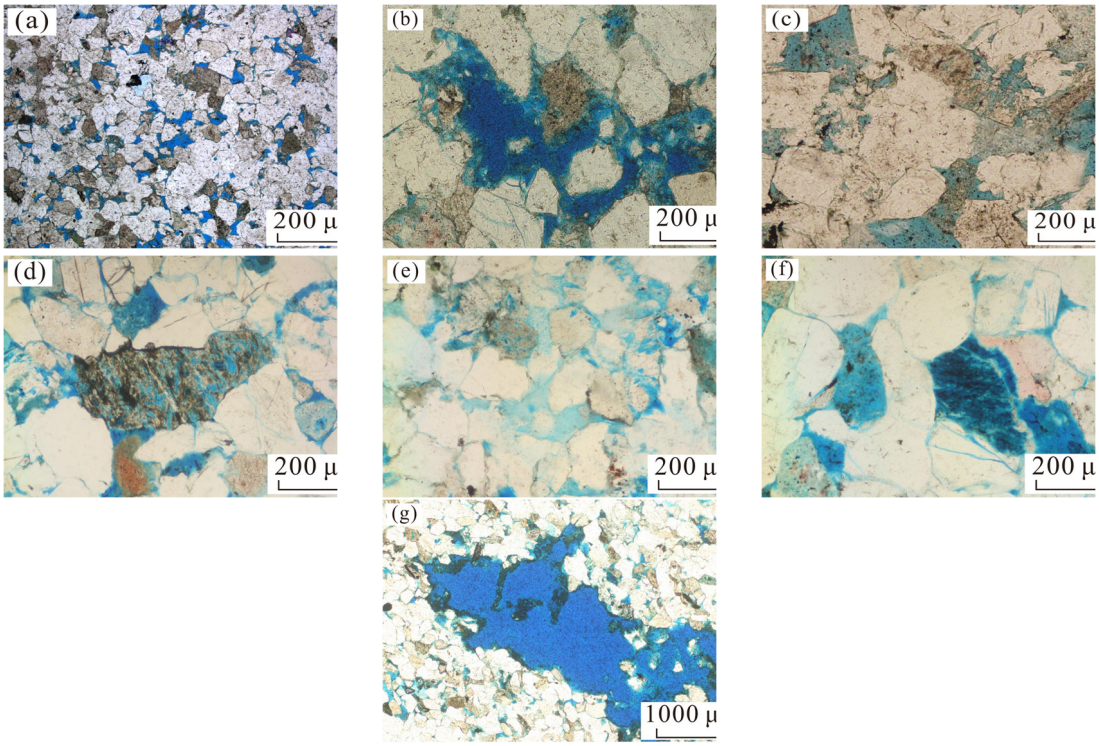

(a) residual intergranular pore, Q, 4222.0m, plane-polarized light; (b) intergranular dissolved pore, Y, 4392.54m, plane-polarized light; (c) the interior of feldspar is dissolved, M, 4055.76m, plane-polarized light; (d) rock debris particles dissolved pore, Y, 4055.76m, plane-polarized light; (e) Filler micropores, Y, 4097.5m, plane-polarized light; (f) the particles are completely dissolved, mol-dic pore, Y, 4391.50m, plane-polarized light; (g) locally see the cave, Y, 4187.5m plane-polarized light.

Figure 4. SEM photomicrographs of the pores occurred in the H formation of the K structure in the eastern X depression

3.2. Pore radius and distribution characteristics

Type I sandstones have a displacement pressure of less than 0.1 MPa, with an average maximum mercury saturation of 80.22% and a peak value of 85.53%, while the residual mercury saturation ranges from 64.21% to 76.92%. The pore-throat radius varies significantly, with an average range of 2.28–5.60 μm, a maximum of 7.36–16.67 μm, and a sorting coefficient between 4.78 and 5.25. Additionally, these sandstones exhibit an average porosity of 12.93% and an average permeability of 32.50×10^{-3} μm², demonstrating good reservoir properties (Fig.5-a).

Type II sandstones have a displacement pressure ranging from 0.13 to 0.48 MPa, with maximum mercury saturation between 67.91% and 86.67%, and an average residual

mercury saturation of 66.05%. The average pore-throat radius is 1.34 μm, with a maximum pore-throat radius around 3 μm, and the sorting coefficient is less than that of Type I sandstones. The samples have an average porosity and permeability of 12.93% and 2.45×10^{-3} μm², respectively (Fig.5-b).

The displacement pressure of Type III samples ranges from 0.32 to 0.78 MPa, with an average maximum mercury saturation of 78.68%. The average pore-throat radius ranges from 0.31 to 4.51 μm, with a maximum pore-throat radius of less than 2.27 μm, and a sorting coefficient between 2.31 and 4.17. These samples have a relatively low porosity, with an average value of only 9.47%, and an average permeability of 0.58×10^{-3} μm² (Fig.5-c).

Type IV samples have a displacement pressure greater than 1 MPa, with an average maximum mercury saturation of 76.71%, and residual mercury saturation ranging from 37.03% to 66.46%. The average pore-throat radius ranges from 0.20 to 3.18 μm, with a maximum pore-throat radius of less than 0.71 μm, and a sorting coefficient of less than 4.06. This type of sandstone has an average porosity of only 7.84% and an average permeability of 0.18×10^{-3} μm² (Fig.5-d).

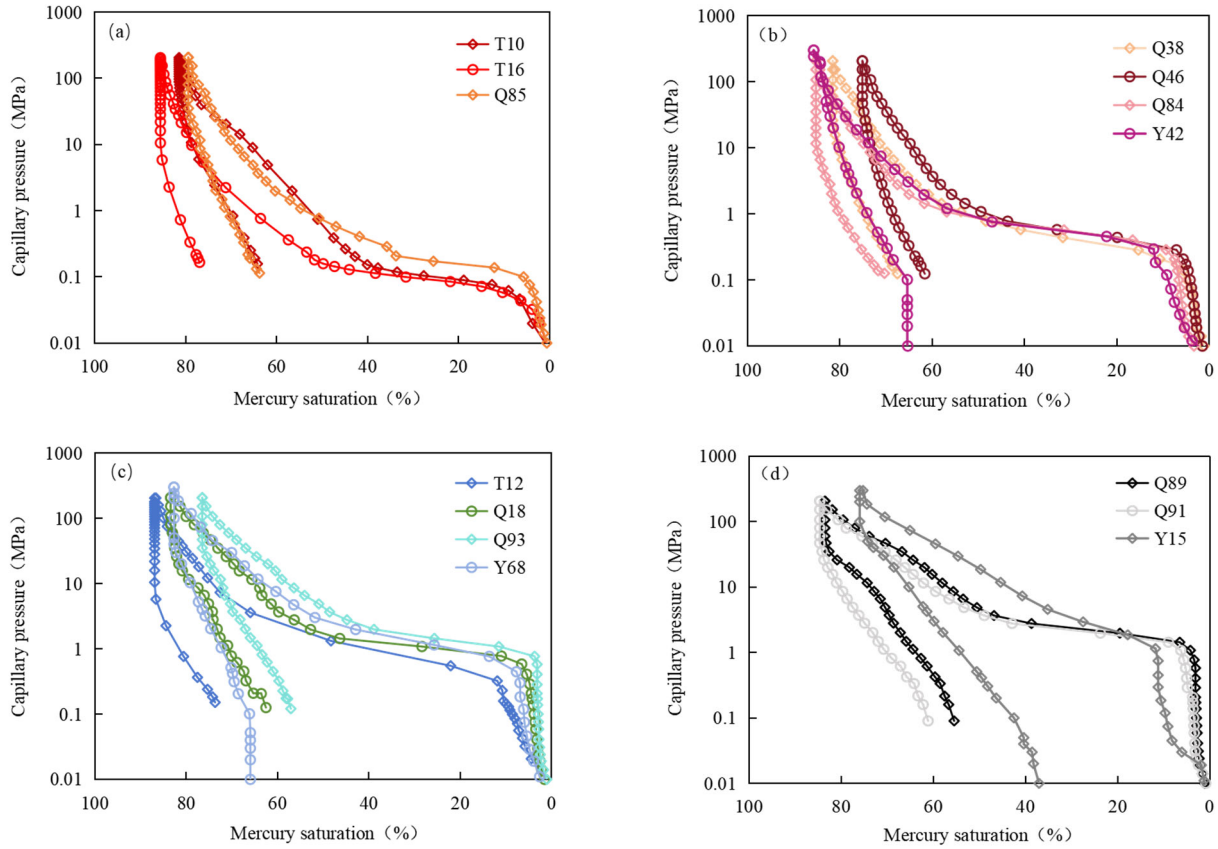

Figure 5. Capillary pressure curve of different types of reservoirs

The average pore-throat radius of the H sandstone group in the K structure of the eastern X depression ranges from 0.209 to 5.426 μm, with significant differences in pore-throat radius distribution among different samples. From type I to type IV reservoirs, the permeability of the samples gradually decreases, the main peak of the pore-throat radius distribution shifts to the right, and the distribution range narrows. This indicates that the pore-throat radius distribution in the study area is relatively complex, with pore-throats of various scales, resulting in strong reservoir heterogeneity.

The pore-throat distribution curve of type I reservoirs is generally skewed to the left, characterized by single or double peaks, with the highest at 6.22 μm and the right peak ranging from 1.38 to 2.12 μm, corresponding to the best physical properties and permeability greater than 10 mD (Fig.6-a). The pore-throat distribution curve of type II reservoirs shifts more to the right compared to type I, with pore-throat radii ranging from 0.62 to 1.85 μm and permeability ranging from 1 to 10 mD (Fig.6-b). For type III reservoirs, the peak of the pore-throat distribution curve tends to shift toward smaller values, with pore-throat radii distributed between 0.32 and 1.64 μm and permeability ranging from 0.2 to 1.0 mD (Fig.6-c). Type IV reservoirs exhibit double or triple peaks in their pore-throat distribution, with radii primarily distributed between 0.006 and 0.426 μm. The left peak is located between 0.222 and 0.426 μm, while the right peak occurs between 0.007 and 0.026 μm, corresponding to the poorest physical properties and permeability generally less than 0.2 mD (Fig.6-d).

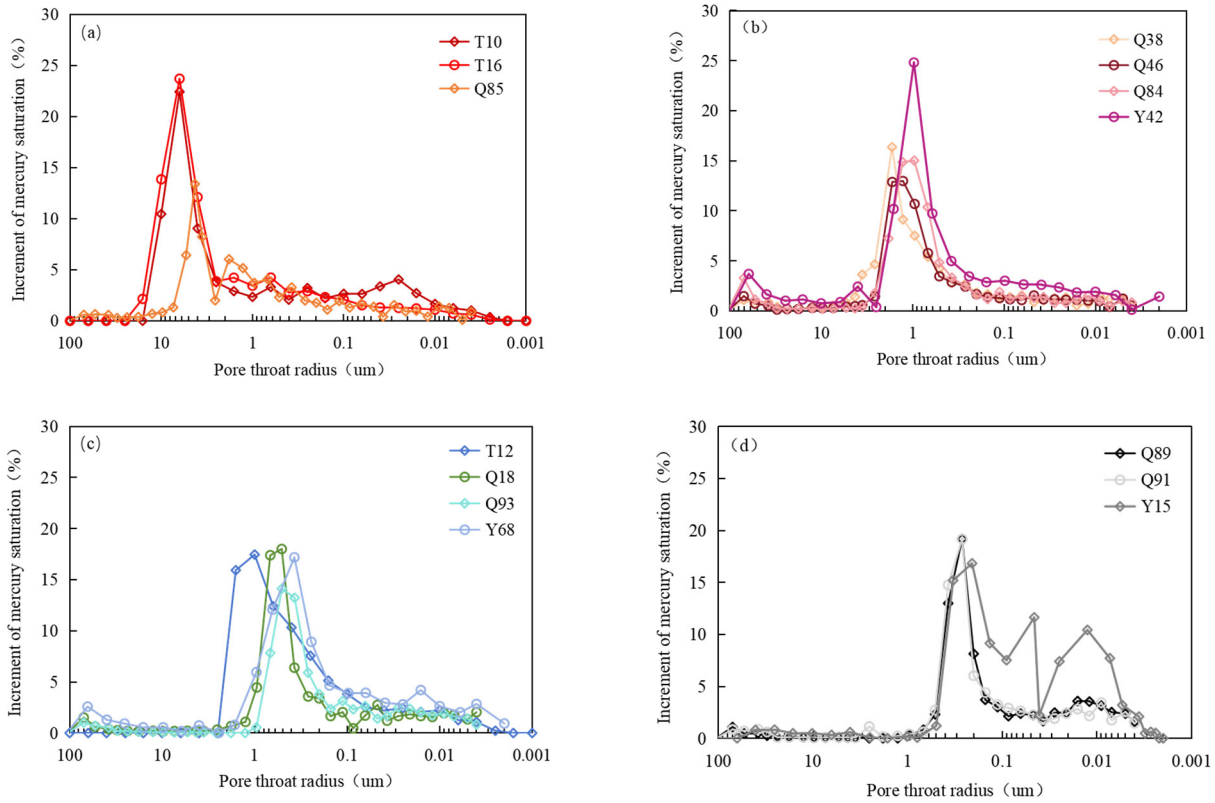

Figure 6. Pore throat distribution of different types of reservoirs

Table 1. Pore throat structure parameters of different types of reservoirs

Parameter		Type I		Type II		Type III		Type IV	
		Range	Average value	Range	Average value	Range	Average value	Range	Average value
Physical parameters	Porosity (%)	10.50~15.80	12.93	8.20~18.90	11.36	4.10~13.39	9.47	5.40~9.20	7.84
	Permeability ($\times10^{-3}$um^2)	11.80~60.60	32.50	1.10~8.14	2.45	0.21~1.00	0.58	0.16~0.19	0.18
Porosity structure parameters	Displacement pressure (MPa)	0.04~0.10	0.06	0.13~0.48	0.28	0.32~0.78	0.56	1.08~3.18	1.61
	Median pressure (MPa)	0.16~1.24	0.68	0.77~3.31	1.53	1.27~14.65	3.52	4.10~19.02	7.69
	Sorting coefficient	4.78~5.25	5.02	2.73~4.25	3.48	2.31~4.17	3.21	2.92~4.06	3.19
	Skewness	0.46~0.74	0.61	-0.09~1.89	0.86	-0.92~1.92	0.81	0.93~1.17	1.05
	Maximum mercury saturationSmax (%)	73.71~88.53	82.22	67.91~86.67	80.42	54.92~85.88	78.68	75.23~85.38	76.71
	The residual mercury saturation (%)	64.21~76.92	70.56	23.35~88.33	66.05	36.03~77.25	65.95	37.03~66.46	57.34
	Average pore throat radius (μm)	2.28~5.60	4.16	0.51~5.00	1.34	0.31~4.51	1.16	0.20~3.18	1.07
	Maximum pore throat radius (μm)	7.36~16.87	12.02	1.81~5.33	3.16	0.94~2.27	1.43	0.65~0.71	0.68

4. Discussion

4.1. Fractal characteristics

Based on the capillary pressure curve, a scatter plot illustrating the relationship between lg(1-S_{Hg}) and lg(P_c) for all samples was constructed (Fig.7). The comparison of fractal characteristics at different pore throat scales demonstrated excellent curve fitting for each segment, indicating that the sandstone samples overall exhibit multifractal properties that can be characterized using fractal geometry theory.

According to the pore classification standard, the effective pore space types are divided into megapores (≥10nm), macropores (2.5-10nm), mesopores (0.5-2.5nm), micropores (0.1-0.5nm) and nanopores (≤0.1nm)[13].

The fractal dimensions D_1, D_2, and D_3 corresponding to megapores and macropores, mesopores, micropores and nanopores were respectively calculated, and the results showed that the range of fractal dimensions for each segment was between 2 and 3, with high correlation as indicated by a coefficient of determination greater than 0.8. D_1 is significantly greater than D_2 and D_3, indicating that larger pore spaces exhibit stronger heterogeneity and a more dispersed pore distribution. The weighted average of mercury saturation values for three different levels of pores can yield the overall fractal dimension of the pore throats. Calculations show that the D_P value ranges from 2.45709 to 2.73181, with an average of 2.59336, indicating that the pore throat structure in the study area is complex and highly heterogeneous.

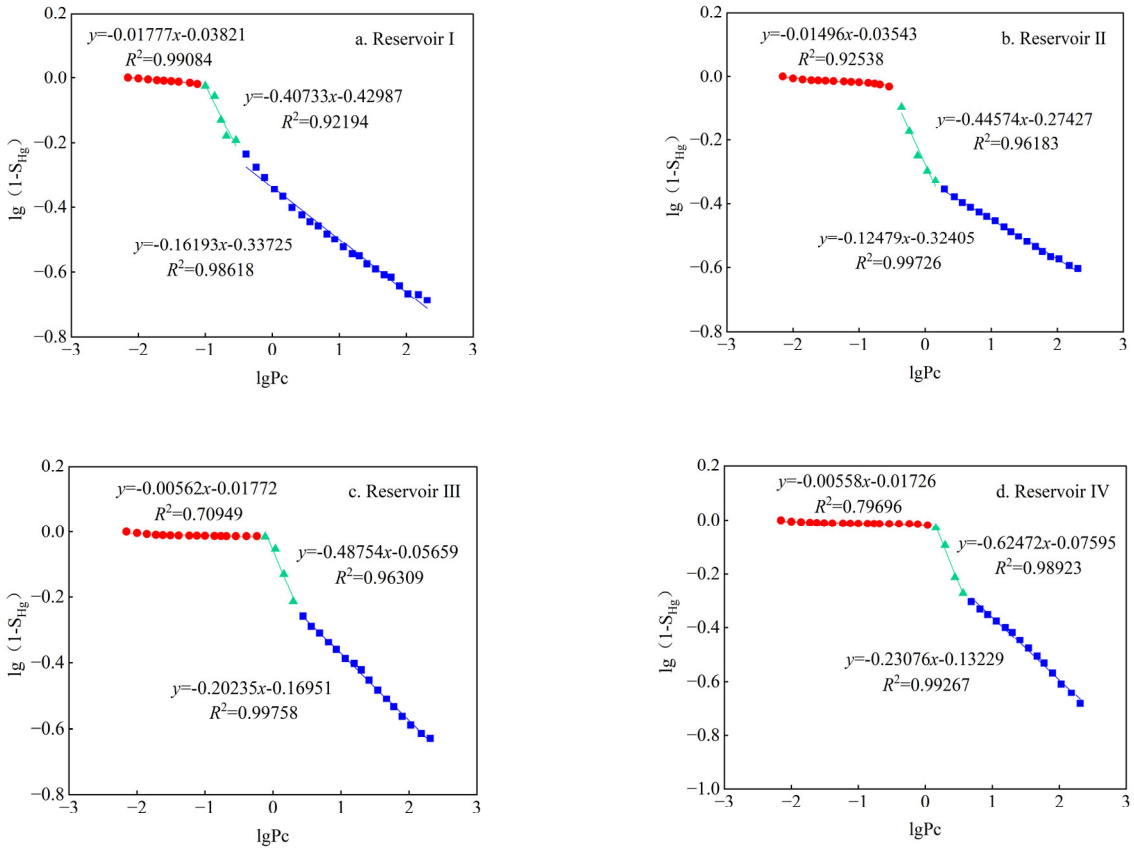

Figure 7. The porefractal characteristics of different types of reservoirs

Table 2. Fitting results of fractal characteristics in different pore intervals

Sample Number	Megapore、Macropore		Mesopore		Micropore、Nanopore		D_P
	D_1	R_2	D_2	R_2	D_3	R_2	
1	2.98876	0.93504	2.24421	0.97162	2.66533	0.97825	2.45709
2	2.98864	0.93017	2.18809	0.98359	2.78655	0.98801	2.51268
3	2.98751	0.96707	2.31141	0.97874	2.76119	0.98361	2.53517
4	2.99438	0.70949	2.59609	0.93903	2.79504	0.99721	2.63534
5	2.99466	0.86246	2.41681	0.94974	2.70898	0.99214	2.57501
6	2.99264	0.76564	2.42738	0.91571	2.57947	0.95823	2.54356
7	2.99401	0.87853	2.34336	0.94449	2.71242	0.99913	2.56077
8	2.99318	0.87768	2.40843	0.92399	2.73655	0.99449	2.61052
9	2.99318	0.87768	2.50843	0.92399	2.73655	0.99449	2.6144
10	2.9934	0.82786	2.38846	0.90383	2.80449	0.99253	2.53713
11	2.99911	0.79949	2.97403	0.93069	2.79896	0.97325	2.72515
12	2.99703	0.82266	2.96988	0.95155	2.7958	0.98198	2.73181
13	2.99895	0.89982	2.97417	0.97589	2.74034	0.97146	2.67512
Average value	2.99349	0.85796	2.51928	0.94560	2.74012	0.98498	2.59336

4.2. The relationship between physical property and fractal dimension

A correlation analysis between the fractal dimensions of the pore structure and porosity, permeability data of the H group reservoir in the K structure of the eastern X depression shows no significant correlation between fractal dimensions and porosity, but there is a good negative correlation between the total fractal dimension D_P of the pore structure under high-pressure mercury intrusion and permeability (Fig.8-a). This indicates that the larger the fractal dimension, the more complex the reservoir pore structure, the lower the permeability, and the stronger the heterogeneity of the reservoir. There is a good negative correlation between the fractal dimensions D_1 of macropores and mesopores, D_2 of mesopores, and their corresponding permeabilities (Fig.8-b,8-c). However, there is no correlation between the fractal dimension D_3 of micropores and nanopores and their corresponding permeabilities (Fig.8-d). This indicates that the contribution to permeability is mainly from macropores and mesopores.

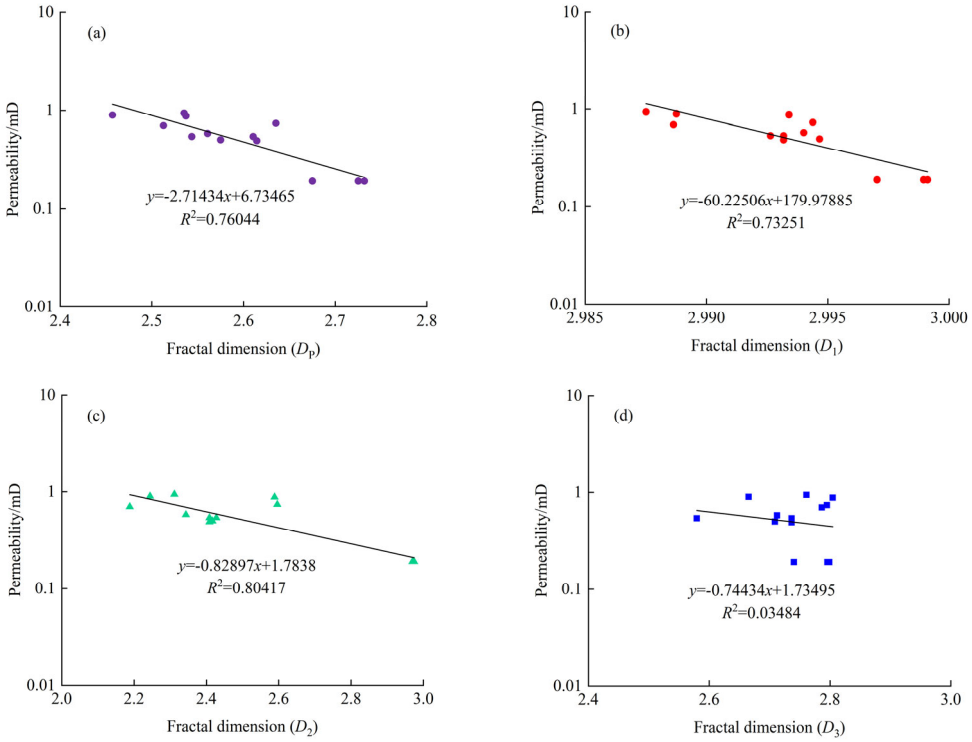

Figure 8. The relationship between physical property and fractal dimension in the H formation of the K structure in the eastern X depression

4.3. The relationship between porosity structure parameters and fractal dimension

To explore the relationship between fractal dimensions and pore structure parameters, the total fractal dimension (D_P), the fractal dimension of macropores and mesopores (D_1), the fractal dimension of mesopores (D_2), and the fractal dimension of micropores and nanopores (D_3) were fitted to the pore structure parameters. Displacement pressure, which refers to the minimum pressure required for the non-wetting phase to displace the wetting phase, serves as a crucial indicator of rock reservoir performance. A strong positive correlation exists between displacement pressure and D_P, D_1, and D_2, where larger fractal dimensions correspond to higher displacement pressures (Fig.9-a). The average pore-throat radius, representing the mean radius of throats, shows a strong negative correlation with D_P, D_1, and D_2 but a weaker correlation with D_3 (Fig.9-b). Smaller fractal dimensions of macropores and mesopores result in a more regular pore structure distribution and reduced heterogeneity. Similarly, the sorting coefficient exhibits a significant positive correlation with D_P, D_1, and D_2, illustrating that the heterogeneity of macropores and mesopores greatly impacts reservoir sorting (Fig.9-c). Larger fractal dimensions lead to poorer concentration in pore-throat distribution, higher sorting coefficients, and more uneven distribution.

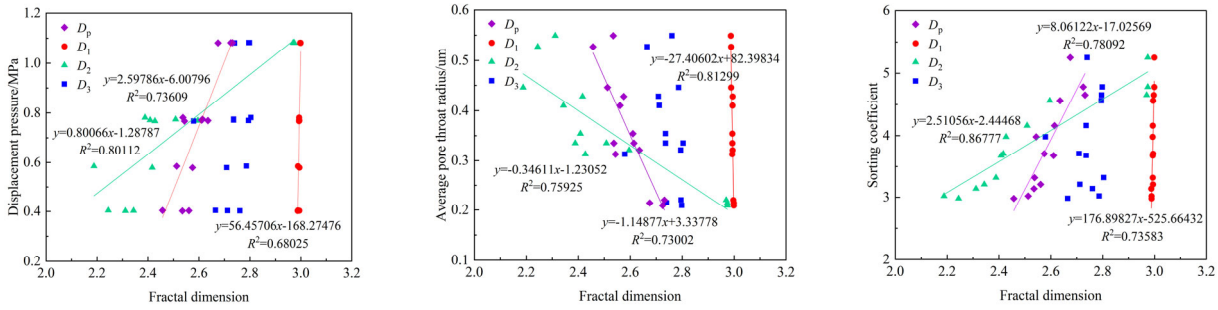

Figure 9. The relationship between physical property and fractal dimension in the H formation of the K structure in the eastern X depression

4.4. The relationship between mineral composition and fractal dimension

To further explore the factors influencing fractal dimensions, the relationship between the relative contents of quartz, feldspar, and chlorite and the fractal dimensions was analyzed. The analysis indicates a negative correlation between D_P, D_1, D_2, and quartz content, suggesting that quartz content affects the heterogeneity of macropores and mesopores (Fig.10-a). Higher quartz content can inhibit compaction to some extent, preserve intergranular pores in the reservoir, and improve the connectivity between pores and throats. D_P and D_2 exhibit a strong negative correlation with feldspar content, while the correlations with D_1 and D_3 are

weaker (Fig.10-b). This indicates that the pore structure heterogeneity of mesopores is related to feldspar content. Feldspar dissolution in the reservoir can create dissolution pores, increasing pore space and enhancing the reservoir's permeability. Chlorite content shows a strong positive correlation with fractal dimensions; higher chlorite content results in larger fractal dimensions and greater reservoir heterogeneity (Fig.10-c). Numerous needle-like chlorite structures are observed filling intergranular pores in the reservoir, with irregular distribution. This affects pore density and distribution patterns, thereby contributing to increased reservoir heterogeneity and a more complex overall pore structure.

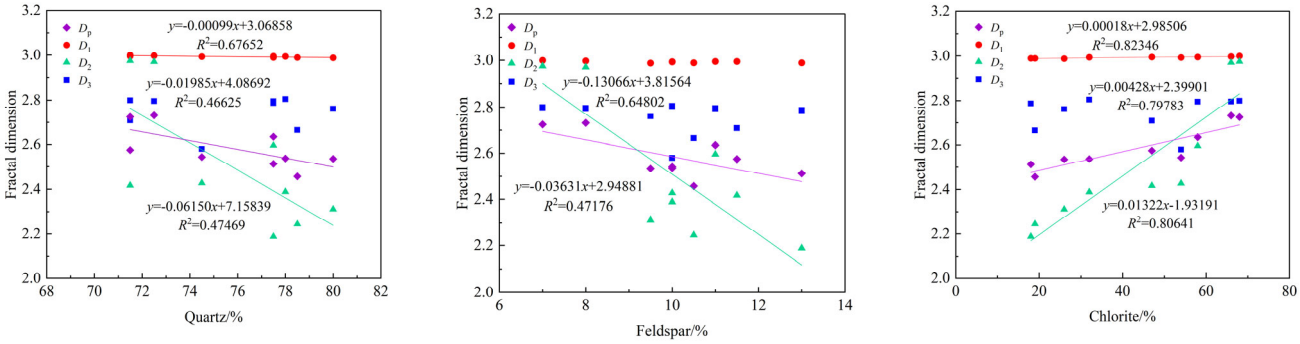

Figure 10. The relationship between mineral composition and fractal dimension in the H formation of the K structure in the eastern X depression

5. Summary

(1) The main pore types of the H reservoir in the K structure of the eastern X depression include primary intergranular pores, intergranular dissolution pores, and intragranular dissolution pores. Its effective reservoir space is mainly composed of megapores, macropores, and mesopores, with significant differences in the distribution frequency of pores and throats of various sizes. The pore-throat structure characteristics are primarily influenced by the development of megapores, macropores, and mesopores.

(2) In terms of heterogeneity and distribution discreteness, the megapores and macropores in the H sandstone reservoir of the study area are larger than the mesopores, micropores, and nanopores. The average total fractal dimension is 2.59336, indicating that the pore-throat structure in the H reservoir is quite complex with strong heterogeneity.

(3) There is a strong negative correlation between the fractal dimension of pore-throats in the H sandstone reservoir and permeability in the study area, with larger pore-throats making a greater contribution to the reservoir's properties. The study indicates that permeability in the H reservoir is primarily influenced by megapores, macropores, and mesopores.

(4) Displacement pressure and sorting coefficient are negatively correlated with the total pore size fractal dimension, whereas the average pore-throat radius shows a positive correlation.

(5) The quartz and feldspar content show a negative correlation with the total pore size fractal dimension, while chlorite content is positively correlated with it. Quartz content mainly influences the fractal dimension of megapores, macropores, and mesopores. Feldspar content primarily affects the fractal dimension of mesopores, and chlorite content mainly influences the fractal dimension of megapores, macropores, and mesopores.

References

[1] JIA Chengzao, PANG Xiongqi, JIANG Fujie. Research status and development directions of hydrocarbon resources in China[J]. Petroleum Science Bulletin, 2016, 1(1): 2-23.

[2] SUN Longde, ZOU Caineng, ZHU Rukai, et al. Formation, distribution and potential of deep hydrocarbon resources in China[J]. Petroleum Exploration and Development, 2013, 40(6): 641-649.

[3] LIU Hongying, LI Jiqiu. Distribution of micro-nano pore throat and its influence on seepage in low permeability and tight oil reservoir[J]. Unconventional Oil & Gas, 2023, 10(3): 98-102.

[4] WANG Yueyun, YU Bingsong, SHEN Zhenhuanu. Quantitative characterization of complexity of sandstone pore-throat structure and its influence on permeability: A case study from Shahejie Formation of Dongying sag[J]. Petroleum Geology and Recovery Efficiency, 2022, 29(5): 39-48.

[5] WANG Xinguang, HUAN Jinlai, PENG Xiaodong, et al. Flow mechanism and pore structures of tight sandstone based on digi tal core analysis[J]. Petroleum Geology and Recovery Effi ciency, 2022, 29(6): 322-30.

[6] WU Hao, LIU Ruie, JI Youliang, et al. Fractal characteristics of pore-throat of tight gas reservoirs and its relation with percolation: a case from He 8 member of the Permian Xiashihezi Formation in Ordos Basin[J]. Acta Sedimentologica Sinica, 2017, 35(1): 151-162.

[7] MANDELBROT B B. The fractal geometry of nature[J]. American Journal of Physics, 1983, 51(3): 286-288.

[8] Xiaozhe, ZHU Haihua. Micro-pore structure and fractal characteristics of the Xiashihezi Formation tight sandstone reservoirs in Sulige area, Ordos Basin[J]. Geological Science and Technology Information, 2019, 38(3): 147-156.

[9] JIANG Rongrong, LI Tao, Yan Huanrong, et al. pore-throat characteristics and percolation capacity of Jurassic tight sandstone reservoirs, western Sichuan Basin[J]. Natural Gas Exploration and Development, 2018, 41(2): 63-69.

[10] ZHANG Quanpei, WANG Haihong, LIU Meirong, et al. Study of the full pore size distribution and fractal characteristics of ultra-low permeability reservoir[J]. Journal of China University of Mining & Technology, 2020, 49(6): 1137-1149.

[11] ZHAO Huitao, GUO Yinghai, DU Xiaowei, et al. Micro-pore multi fractal characteristics of Benxi formation sandstone reservoir in Gaoqiao area, Ordos basin[J]. Bulletin of Geological Science and Technology, 2020, 39(6): 175-184.

[12] FAN Xuqiang, WANG Guiwen, LI Yafeng, et al. Pore structure evaluation of tight reservoirs in the mixed siliciclastic-carbonate sediments using fractal analysis of NMR experiments and logs[J]. Marine and Petroleum Geology, 2019, 109: 484-493.

[13] HARTMANN D J, BEAUMONT E A. Predicting reservoir system quality and performance[C]//BEAUMONT E A, FOSTER N H. Exploring for Oil and Gas Traps, AAPG Treatise of Petroleum Geology, Handbook of Petroleum Geology. Tulsa: AAPG, 1999: 438-456.